Smart Multifunctional Nanostructure for Targeted Cancer Chemotherapy and Magnetic Resonance Imaging

Tao Chen,[†] Mohammed Ibrahim Shukoor,[†] Ruowen Wang,[†] Zilong Zhao,[†,‡] Quan Yuan,[†,‡] Suwussa Bamrungsap,[†] Xiangling Xiong,[†] and Weihong Tan[†,‡,*]

[†]Center for Research at Bio/Nano Interface, Department of Chemistry and Department of Physiology and Functional Genomics, Shands Cancer Center, UF Genetics Institute and McKnight Brain Institute, University of Florida, Gainesville, Florida 32611-7200, United States, and [‡]State Key Laboratory for Chemo/Biosensing and Chemometrics, College of Biology, College of Chemistry and Chemical Engineering, Hunan University, Changsha 410082, People's Republic of China

ABSTRACT Targeted chemotherapy and magnetic resonance imaging of cancer cells *in vitro* has been achieved using a smart multifunctional nanostructure (SMN) constructed from a porous hollow magnetite nanoparticle (PHMNP), a heterobifunctional PEG ligand, and an aptamer. The PHMNPs were prepared through a three-step reaction and loaded with the anticancer drug doxorubicin while being functionalized with PEG ligands. Targeting aptamers were then introduced by reaction with the PEG ligands. The pores of the PHMNPs are stable at physiological pH, but they are subject to acid etching. Specific binding and uptake of the SMN to the target cancer cells induced by aptamers was observed. In addition, multiple aptamers on the surface of one single SMN led to enhanced binding and uptake to target cancer cells due to the multivalent effect. Upon reaching the lysosomes of target cancer cells through receptor-mediated endocytosis, the relatively low lysosomal pH level resulted in corrosion of the PHMNP pores, facilitating the release of doxorubicin to kill the target cancer cells. In addition, the potential of using SMN for magnetic resonance imaging was also investigated.

KEYWORDS: aptamer · chemotherapy · doxorubicin · magnetic resonance imaging · nanostructure

Since most anticancer drugs are unable to differentiate between diseased and healthy cells, systemic toxicity and undesired side effects can result.[1] However, these issues can be addressed through tumor-specific delivery of anticancer drugs using nanostructures equipped with targeting moieties.[2] Many tumors possess fenestrated vasculature and poor lymphatic drainage because of their rapid growth. At the same time, an enhanced permeability and retention (EPR) effect results,[3] allowing nanostructures to accumulate specifically at the tumor site by the mechanism of passive targeting. In addition, tumor localization of nanostructures can be further enhanced by active targeting groups that have molecular recognition to target cancer cells, such as the vitamin folic acid,[4,5] peptides,[6,7] and aptamers.[8−14] However, even if a high level of anticancer drugs can reach the tumors, this does not mean that sufficient drug molecules will automatically be taken up by the target cancer cells to effectively kill them.[15,16] Therefore, other than tumor targeting, the ability to induce efficient uptake of anticancer drugs is another important factor to consider when choosing the proper targeting ligand.[17]

Aptamers are single-stranded oligonucleotides that can bind specifically to their targets, which range from small molecules to proteins, whole cells, and even tissues, by folding into distinct secondary or tertiary structures.[14] Generated by a process called SELEX (Systematic Evolution of Ligands by EXponential enrichment) developed in the 1990s,[18,19] aptamers rival antibodies for their molecular recognition ability.[20] Thus, they have emerged as new targeting moieties for biotechnological and therapeutic applications. Recently, our group has developed a cell-based SELEX strategy that can produce a panel of aptamers for cancer cells.[21,22] In addition to specific binding to cancer cells, some of these aptamers can be internalized into cancer cells,[23] thus making them good candidates for intracellular drug delivery.

Among all nanocarriers, smart nanostructures that are responsive to external stimuli, such as heat,[24] light,[25] or acidic conditions,[26] have attracted the attention of researchers. By formulating these smart nanostructures with imaging contrast agents, an all-in-one system combining tumor targeting, tumor therapy, and tumor imaging is possible.[27−29] In this study, a smart multifunctional nanostructure (SMN) was constructed of three components: a porous hollow magnetite nanoparticle (PHMNP) as a carrier, a heterobifunctional PEG ligand as a linker, and an aptamer as a targeting moiety. This nanostructure was successfully utilized for targeted chemotherapy and

* Address correspondence to tan@chem.ufl.edu.

Received for review June 6, 2011 and accepted September 2, 2011.

Published online September 02, 2011
10.1021/nn202073m

magnetic resonance imaging (MRI). The hollow interior of the PHMNPs is loaded with the anticancer drug doxorubicin (DOX). Multiple aptamers on the outer layer of SMN resulted in a multivalent effect, leading to enhanced specific binding and internalization of SMNs to target cancer cells. Because of having acid-labile pores, upon arrival of lysosomes, the acidic environment of the lysosomes facilitated the release of DOX from SMN, enabling efficient killing of target cancer cells. In addition, T_2 relaxation measurements and T_2*-weighted MRI images showed that this nanostructure had great potential to be used as a T_2 contrast agent.

RESULTS AND DISSCUSSION

SMNs were prepared as outlined in Figure 1a. First of all, PHMNPs were obtained through a three-step reaction:[30] First, 13 nm iron-magnetite core–shell nanoparticles (IMNPs) (Figure 1b) were produced by thermal decomposition of iron pentacarbonyl ($Fe(CO)_5$). Second, through controlled oxidation of IMNPs in the presence of the oxygen-transfer reagent trimethylamine N-oxide (Me_3NO), 16 nm hollow magnetite nanoparticles (HMNPs) were obtained. The TEM image (Figure 1c) showed that they have hollow interiors about 10 nm in diameter and magnetite shells around 3 nm in thickness. Third, acid etching of HMNPs in the presence of oleic acid at high temperature resulted in PHMNPs (Figure 1d). The hollow interiors of PHMNPs were encircled with discrete polycrystalline magnetite domains, and the pores of the PHMNPs were 2–4 nm.

The as-prepared PHMNPs are hydrophobic by their oleylamine/oleate coating and have no active functional groups. Therefore, the heterobifunctional PEG ligand with a catechol group on one end and a carboxyl group on the other end was synthesized according to a method reported in the literature[30] with proper modifications (see Supporting Information for detailed synthesis route). The ligands were introduced onto the surface of PHMNPs to make them hydrophilic through ligand displacement. The resultant PEGylated PHMNPs (PPHMNPs) were easily dispersed in aqueous solution as shown in Figure 1e and had a hydrodynamic diameter of around 60 nm. In addition, the heterobifunctional PEG ligand also equipped PPHMNPs with an active carboxyl functional group.

At last, aptamers with an amino group and a desired fluorophore modification were prepared through solid phase synthesis using an automatic DNA synthesizer and anchored onto the surface of PPHMNPs by reacting with the active carboxyl group on the heterobifunctional PEG ligand. In order to avoid any adverse effect on binding specificity and affinity, 10 thymine (T) bases were inserted between the amino group and the aptamer sequence. PPHMNPs do not show

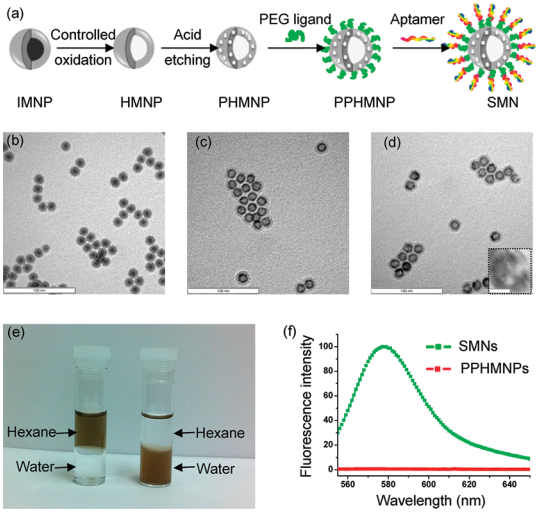

Figure 1. Synthesis and characterization of SMNs. (a) Schematic illustrating the synthesis of SMNs. TEM images of (b) IMNPs; (c) HMNPs; and (d) PHMNPs. Inset of (d) shows the enlarged image of a representative PHMNP. The scale bars are 100 nm (10 nm for the inset). (e) Dispersibility of PHMNPs (left) and PPHMNPs (right) in hexane and water. (f) Fluorescence intensity of PPHMNPs and SMNs (excitation: 545 nm). (IMNP = iron-magnetite core–shell nanoparticle, HMNP = hollow magnetite nanoparticle, PHMNP = porous hollow magnetite nanoparticle, PPHMNP = PEGylated porous hollow magnetite nanoparticle, SMN = smart multifunctional nanostructure).

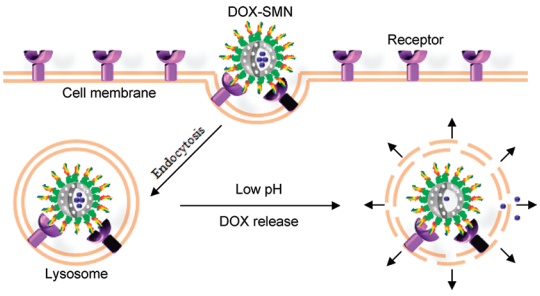

Scheme 1. Mechanism of SMNs for targeted cancer chemotherapy. Due to surface coating of aptamers, DOX-SMNs specifically enter target cancer cells through receptor-mediated endocytosis and reside in acidic lysosomes. This leads to SMN pore size enlargement because of its acid sensitivity, facilitating the release of entrapped DOX and the killing of target cancer cells. (SMN = smart multifunctional nanostructure, DOX-SMN = DOX-loaded SMN, DOX = doxorubicin.)

any fluorescence; however, a strong fluorescence signal was observed for SMNs after the successful introduction of fluorophore-labeled aptamers. Figure 1f shows an example of using carboxytetramethylrhodamine (TAMRA)-labeled aptamers. TAMRA is a commonly used fluoreophore modifier for DNA sequences with emission around 580 nm when excited around 540 nm.

Scheme 1 shows the mechanism of using SMNs for targeted cancer chemotherapy. The anticancer drug DOX was loaded into the hollow cavity of SMNs. Owing to aptamers on the surface of DOX-SMNs, the loaded nanoparticles can specifically bind and then enter

target cancer cells through receptor-mediated endocytosis. Since the pores of SMNs are stable at physiological pH but vulnerable to acidic pH, the low lysosomal pH level will enlarge the pores of SMNs, accelerating the release of DOX from SMNs and the killing of target cancer cells.

In order to have a large loading capacity, drug loading and PEGylation of PHMNPs were performed simultaneously to reduce the barrier effect to a minimal extent. As quantified by measuring the absorbance of DOX at 485 nm, the drug payload was 8.72 wt %. For investigating the release kinetics of DOX loaded into PPHMNPs, the particles were dialyzed against PBS buffer at different pH values (pH = 5, 6, and 7.4). The release of DOX was shown to be a pH-dependent, diffusion-controlled process (Supporting Information, Figure S2). At physiological pH (pH = 7.4), a gradual increase and a plateau were observed after the initial burst of DOX release. The $t_{1/2}$ (the time needed for the release of 50% of the maximal loading) was approximately 21.5 h. For lower pH values, a similar release behavior was observed, albeit with shorter $t_{1/2}$ (7.5 h at pH = 6 and 3.5 h at pH = 5). We attribute the observed pH-dependent release behavior to the low pH environments, which can enlarge the acid-labile pores of PHMNPs to accelerate the rate of DOX release from DOX-loaded PPHMNPs.[30] Thus, the lower the pH value, the faster the release of DOX. Since the oleylamine/oleate layer on the as-prepared PHMNPs is successfully replaced with a layer of the heterobifunctional PEG ligand through ligand displacement as mentioned before, the possibility of DOX release at acidic pHs due to oleic acid protonation can be excluded. In addition, because of the concrete structure of PHMNPs, the probability of DOX entering the nanoparticle matrix during its loading process is very low, and thus it is unlikely that DOX would release from the nanoparticle itself under acidic environments. Although the nitrogen atoms in the heterobifunctional ligand may be protonated at low pH values to alternate the surface charge of PPHMNPs, we believe that this is unlikely to be the reason for DOX release since it is already loaded into the cavity of PPHMNPs. However, the pH-dependent solubility of DOX[31,32] may also play a role in the release kinetics other than acid-etching of the pores. The reported pH in lysosomes[33−35] is between 4.0 and 6.5, which is relatively low compared to the physiological pH of 7.4. Therefore, the release of DOX from SMNs can be achieved inside the lysosomes.

In order to determine if the conjugated aptamer still preserves its binding affinity and specificity, the binding of SMNs toward target and control cancer cells was studied using flow cytometry. Fluorescein isothiocyanate (FITC)-labeled sgc8, which specifically binds to cell membrane receptor protein tyrosine kinase 7 (PTK 7), was used as the targeting aptamer. CEM cells, which have a high expression of PTK 7, were chosen as target cancer cells, whereas Ramos cells with no PTK 7 on the membrane were used as control cancer cells. As shown in Figure 2a, a large shift was observed for CEM cells treated with the SMNs, but no significant shift was observed for Ramos cells (Figure 2b). Corresponding confocal fluorescence microscopy images were consistent with the flow cytometry results (Supporting Information, Figure S3): a strong green fluorescence was observed for CEM cells, but no distinct fluorescence was seen for Ramos cells. Compared with aptamer only, enhanced binding was observed for CEM cells treated with SMNs. As shown in Figure 2c and d, a larger shift was observed in the flow cytometry histograms, even though a smaller number of SMNs was used. This result could be attributed to multivalent interactions, *i.e.*, the simultaneous binding event of multiple aptamers on SMNs to multiple PTK 7 receptors on the cell membrane. Since the affinity of a ligand for its receptor is highly dependent on the three-dimensional arrangement and valency of the targeting moieties,[36] equipping nanocarriers with multiple targeting ligands has become a popular strategy to enhance specific binding affinity to the target cells. The enhanced binding arises from the increased residence time of the ligands on the cell membrane, leading to greater incorporation.[37] Since no binding occurs between Ramos cells and the aptamers on the SMNs, neither shift nor enhancement was observed. Thus, the aptamer still maintains its binding capability toward its target cells after being incorporated onto SMNs.

We next investigated whether SMNs could be internalized into the target cancer cells. Since FITC is a pH-sensitive dye and its fluorescence is greatly reduced in acidic environments, such as in lysosomes inside living cells, the aptamer was labeled with 3′-TAMRA for confocal fluorescence microscopy. After incubating CEM cells with SMNs at 37 °C for 2 h, a strong red fluorescence was observed by confocal fluorescence microscopy, but no distinct red fluorescence was seen for Ramos cells (data not shown). The sgc8 aptamer has previously been reported to enter cells through receptor-mediated endocytosis, with the lysosome as its final destination inside living cells.[23] Therefore, a colocalization study was carried out to determine if the SMNs also entered the lysosomes. While incubating the cells with free aptamer or SMNs, the lysosomes of CEM cells were labeled with a green dye known as lysosensor. From confocal fluorescence microscopy images (Figure 3), a green fluorescence from the lysosensor was observed for the first channel, and a red fluorescence from the aptamer or the SMNs was seen for the second channel. In addition, the images overlapped well and produced a yellow fluorescence inside the CEM cells, indicating that both the aptamer and the SMNs could enter the cells and reside in their lysosomes. In addition, for CEM cells treated with SMNs, even

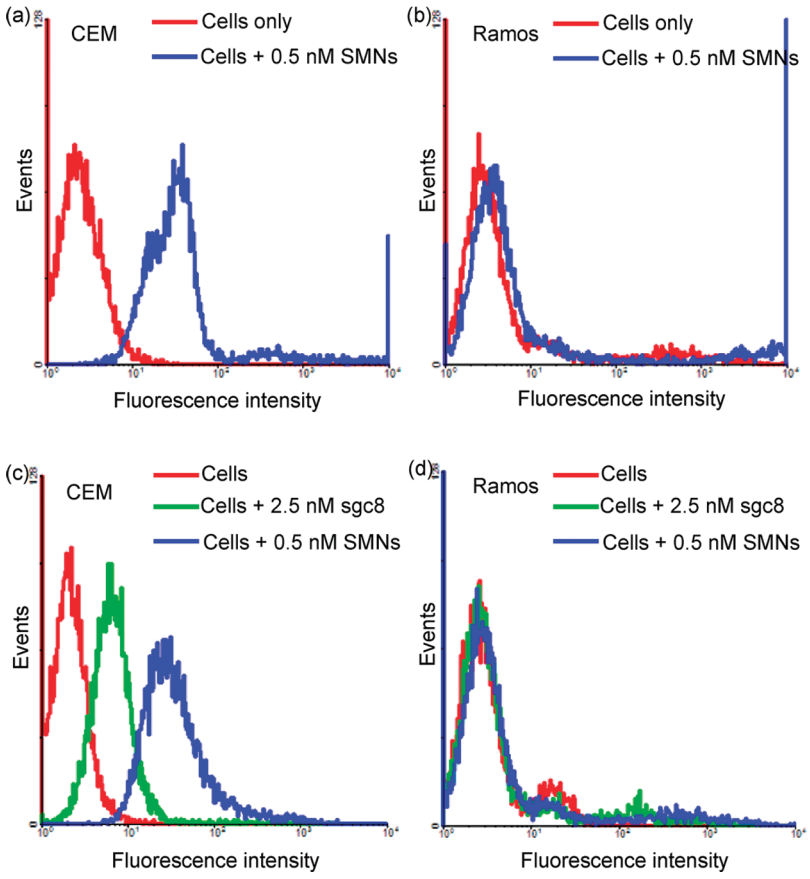

Figure 2. Flow cytometry histograms to monitor the binding of SMNs with (a) CEM cells (target cells) and (b) Ramos cells (control cells). Flow cytometry histograms to compare the binding of free sgc8 aptamer and SMNs with (c) CEM cells and (d) Ramos cells.

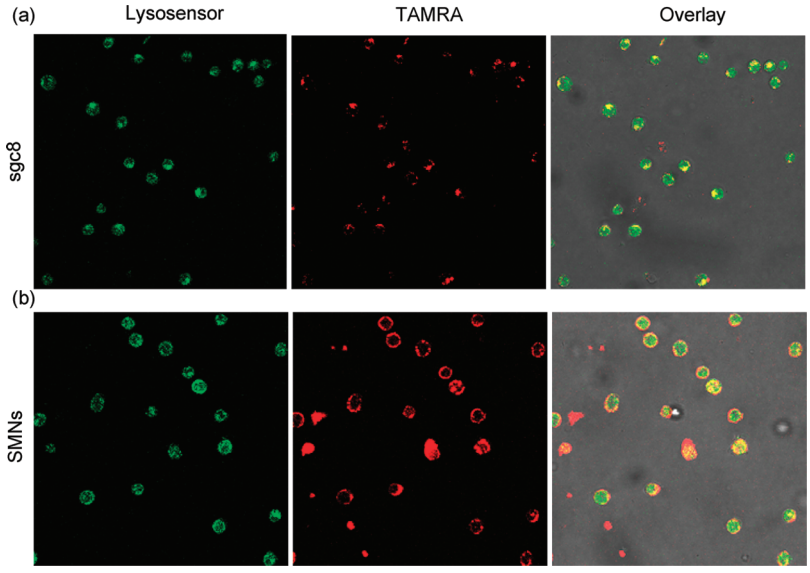

Figure 3. Co-localization study of (a) sgc8 aptamer and (b) SMNs with lysosensor in CEM cells (target cells).

though a similar green fluorescence was observed compared with cells treated with free aptamer, a much stronger red fluorescence was seen with the concentration of SMNs at 1 nM and aptamer at 5 nM, indicating an improved uptake efficiency of SMNs to target cancer cells, which is most likely attributed to multivalent binding. This enhanced internalization and the low pH inside lysosomes, coupled with the instability of SMN pores in an acidic environment, should facilitate the release of the anticancer drug efficiently.

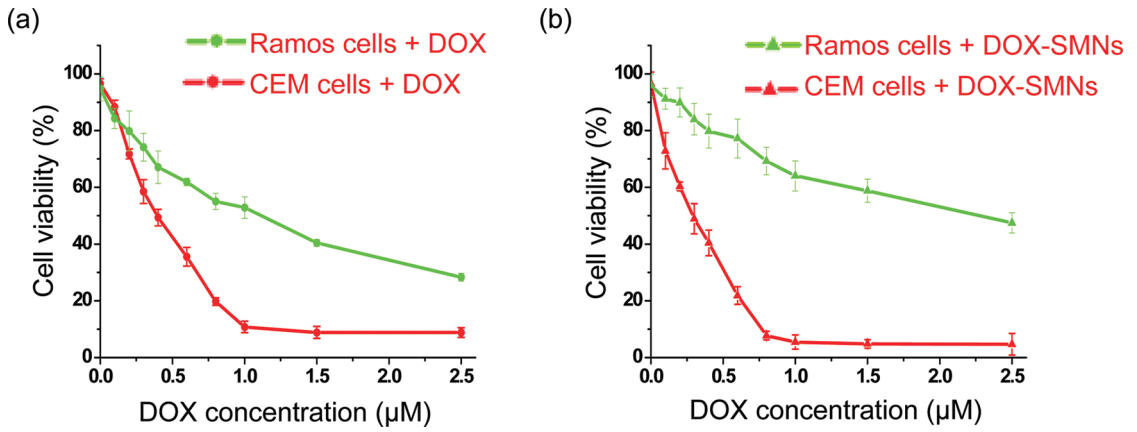

Figure 4. Cytotoxicity assay of CEM cells (target cells) and Ramos cells (control cells) treated with (a) DOX only and (b) DOX-SMNs.

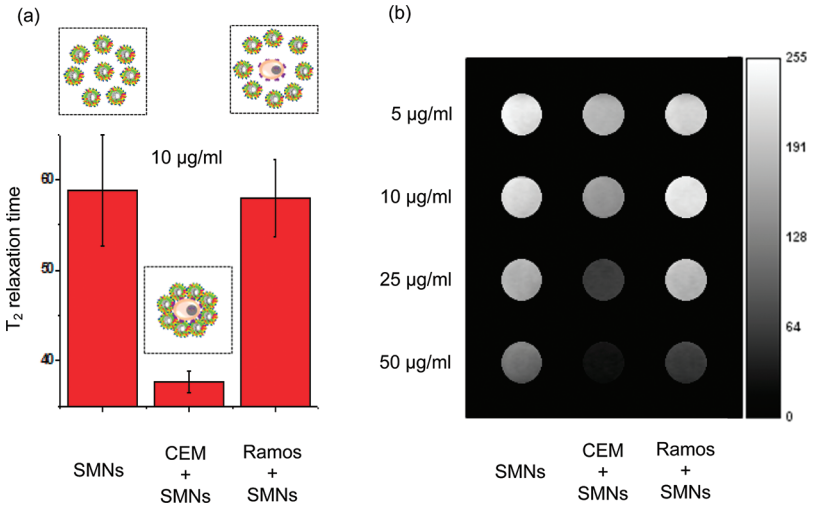

Figure 5. Potential of using SMNs as T_2 contrast agents. (a) T_2 relaxation measurements and (b) T_2*-weighted MRI images of SMNs, SMNs incubated with CEM cells (target cells), and SMNs incubated with Ramos cells (control cells). The concentration of SMNs in (a) is 10 μg/mL, while their concentrations in (b) are labeled on the right side of the figure.

As demonstrated by a release kinetics study, SMNs loaded with DOX show slow release of drug under physiological conditions, but rapid release in acidic environments, such as that found in lysosomes. Therefore, the high specificity of aptamers to their target cells should allow efficient and selective cytotoxicity to CEM cells. To prove this point, the *in vitro* cytotoxicities of SMNs only, DOX-SMNs, and DOX only to both CEM and Ramos cells were investigated. Since magnetite-based magnetic nanoparticles (MNPs) possess excellent biocompatibility, a negligible effect of SMNs only on both cell lines was observed (Supporting Information, Figure S4). For DOX only and DOX-SMNs (Figures 4a and b, respectively), they presented dose-dependent cytotoxicity behavior to CEM as well as Ramos cells. Compared to the IC_{50} of DOX only (0.39 μM) to CEM cells, a smaller IC_{50} of 0.27 μM was obtained for DOX-SMNs, showing the enhanced killing efficacy of DOX-SMNs. However, for Ramos cells, relatively weak drug potency of DOX-SMNs was seen, which can be attributed to two possible reasons: (1) there is minimal internalization of DOX-SMNs to Ramos cells and (2) DOX release from DOX-SMNs to binding buffer (leaking) is small during the 2 h cell treatment. In addition, around 50% of Ramos cells were killed by DOX only when its dose (*e.g.*, 0.8 μM) was sufficient to kill more than 80% of CEM cells. However, only around 20% of Ramos cells were killed when more than 80% of CEM cells were killed by DOX-SMNs (*e.g.*, 0.6 μM), demonstrating the superior selectivity of DOX-SMNs compared to conventional chemotherapy using DOX only. Summarizing the results from the cytotoxicity assay, one can easily draw the conclusion that enhanced killing efficacy and improved targeting specificity can be achieved by using SMNs. One factor that needs to be pointed out is that the cytotoxicity behavior difference between CEM and Ramos cells to DOX only resulted from their distinct susceptibilities to the drug.[12]

Most biological samples exhibit virtually no magnetic background; therefore, MNPs have been used for highly sensitive measurements and superior contrast imaging in turbid or otherwise visually obscured

samples without purification, allowing for rapid assays. For magnetite-based MNPs, the transverse (or spin−spin) relaxation time (T_2) is typically used for biosensing and MRI applications, since their transverse relaxivity is significantly larger than longitudinal relaxivity. Here, we investigated the potential of using SMNs for MRI. The imaging strategy is based on a self-amplifying proximity assay using SMNs.[38] When many SMNs bind to their intended molecular target through the interaction between the receptors on target cancer cell membrane and the aptamers on SMNs, they act cooperatively to form microscale clusters. According to outer-sphere theory, the relaxivity of a particle is directly proportional to its cross-sectional area.[39,40] Consequently, when SMNs assemble into clusters in the presence of their target cancer cells, the effective cross-sectional area increase exceeds the additive contribution from all SMNs on the cell membrane, resulting in a larger and more powerful magnetic dipole. This makes the aggregated SMNs more efficient in enhancing the net transverse relaxation of neighboring water protons, leading to a decreased T_2.

Using a benchtop nuclear magnetic resonance relaxometer, we quantified the T_2 of surrounding water protons in SMNs only, SMNs incubated with CEM cells, and SMNs incubated with Ramos cells. Compared with SMNs only, SMNs treated with CEM cells showed a huge decrease in the T_2 of the surrounding water protons, while SMNs treated with Ramos cells showed no obvious change (Figure 5a). As an intended molecular target for SMNs, PTK 7 receptor is highly expressed on CEM instead of Ramos cells. Therefore, effective cluster formation of SMNs and decreased T_2 of surrounding water protons are expected in the sample containing CEM cells, but not the Ramos cell sample. When a reversible bulk field dephasing effect caused by local field inhomogeneities is incorporated into T_2, its characteristic time is referred to as T_2*. Compared to T_2-weighted MRI images, T_2*-weighted MRI images have better contrast, since they exhibit considerably higher sensitivity to susceptibility differences.[41] Therefore, T_2*-weighted MRI images of SMNs only, as well as SMNs incubated with CEM and Ramos cells, were further obtained at four different SMN concentrations, and the results are shown in Figure 5b. Comparing the first column (SMNs only) and the third column (SMNs treated with Ramos cells), similar darkness was seen since there is no specific interaction between Ramos cells and SMNs. However, much darker images were obtained for the second column (SMNs treated with CEM cells), consistent with the relaxation measurements. Putting the T_2 relaxation measurements and T_2*-weighted MRI images together, we demonstrated that the SMNs could specifically bind to their target cancer cells, effectively forming clustered structures, resulting in decreased T_2 and additional image contrast.

CONCLUSIONS

In summary, our pH-sensitive SMNs demonstrated efficient release of anticancer drug at lysosome pH and great potential to be used as T_2 contrast agents. With the incorporation of targeting aptamers onto PHMNPs with acid-labile pores, the resulting drug delivery platform offers several attractive features: (1) rapid release of toxic anticancer drug, (2) enhanced specific binding and cell uptake from the multivalent effect, (3) decreased nonspecific killing of control cancer cells, (4) simultaneous MRI imaging. The improved specificity and internalization of our drug delivery platform and its rapid release of anticancer drug inside cancer cell lysosomes greatly facilitate the treatment of cancer with minimized systemic toxicity. Together with passive targeting from the EPR effect, our drug delivery platform with active targeting from aptamers should have better therapeutic efficacy, especially for *in vivo* cancer treatment. Moreover, the great potential of using SMNs as T_2 contrast agents may enable real-time monitoring of the cancer treatment progress.

MATERIALS AND METHODS

Synthesis of Heterobifunctional PEG Ligand. See Supporting Information for details.

PEGylation of PHMNPs and DOX Loading. A 5 mg sample of PHMNPs dissolved in 5 mL of tetrahydrofuran (THF) was degassed under a blanket of Ar for 15 min and transferred to a dropping funnel. The solution was added dropwise into 75 mg of heterobifunctional PEG ligand dissolved in 15 mL of THF over a period of 6 h under argon. The resultant mixture was stirred under a blanket of Ar at 50 °C overnight. The PPHMNPs were then precipitated by adding hexane and collected by a strong magnet. The collected nanoparticles were washed with 200 μL of PBS buffer three times and then dispersed in ultrapure water or PBS buffer for further use. For DOX loading, a similar experimental procedure was used, but 10 mg of DOX was premixed with 75 mg of heterobifunctionl PEG ligand dissolved in 15 mL of THF. In addition, after the reaction, the solvent was evaporated under low pressure.

Synthesis of Aptamer. The sgc8 aptamers with amino group and desired dye modifications were synthesized on an ABI 3400 DNA/RNA synthesizer (Applied Biosystems, Foster City, CA, USA). The aptamer with FITC labeling was used primarily for flow cytometry, while the aptamer with TAMRA labeling was used for confocal fluorescence microscopy. The aptamer without dye labeling was used for the cytotoxicity assay. Detailed sequence information is provided in the Supporting Information (Table S1). The aptamers with and without FITC labeling were deprotected in 3 mL of AMA solution (ammonium hydroxide:40% aqueous methylamine = 1:1) at 65 °C for 25 min. The TAMRA-labeled aptamers were deprotected in 3 mL of TAMRA deprotection solution (methanol:*tert*-butylamine:water = 1:1:2) at 65 °C for 4 h. All deprotected sequences were precipitated by adding 250 μL of 3 M NaCl and 6 mL of cold ethanol. Then the precipitated aptamers were collected by centrifugation and dissolved in 400 μL of triethylammonium acetate (TEAA) for further purification by reversed-phase high-pressure liquid

chromatography (ProStar, Varian, Walnut Creek, CA, USA) using a C_{18} column and acetonitrile–TEAA solvent. Finally, these aptamers were quantified by measuring their absorbance at 260 nm.

Anchoring of Aptamers onto PPHMNPs. To immobilize aptamers onto PPHMNPs, standard peptide bond-formation methodology was used. To 150 μL of PPHMNPs in PBS buffer with a concentration of 1.5 mg/mL was added 30 μL of 10 mM 1-ethyl-3-(3-dimethylaminopropyl) carbodiimide in PBS buffer. The resultant mixture was incubated at room temperature for 15 min while shaking. Then, 30 μL of 12 mM *N*-hydroxysuccinimide in PBS buffer, 60 μL of 50 μM aptamer in PBS buffer, and 30 μL of PBS buffer were added and further incubated at room temperature for another 1 h. Successfully synthesized SMNs were collected by a strong magnet and washed three times with 200 μL of PBS buffer. Finally, the resultant product was either redispersed in PBS buffer for further use or lyophilized and stored at −20 °C.

DOX Payload Determination and Release Kinetics Study. The DOX payload determination and release kinetics study were carried out using dialysis membrane tubing (MWCO = 3500). The released DOX can cross the dialysis membrane, but not the SMNs. In order to determine the maximal loading of DOX into PHMNPs, 2 mg of DOX-loaded PPHMNPs dispersed in 0.5 mL of PBS buffer in dialysis membrane tubing was floated in 20 mL of PBS buffer (pH = 7.4) at 37 °C. After 72 h, a 200 μL aliquot of the dialyzed buffer was removed, and the absorbance at 485 nm was measured. In order to study the release kinetics of DOX from PPHMNPs, a similar experimental setup with the same temperature and release time was used, but PBS buffers with different pH values (pH = 5, 6, 7.4) were used. Moreover, 200 μL aliquots were removed for absorbance measurement at predetermined time intervals. Each 200 μL aliquot was replaced with 200 μL of fresh PBS buffer to maintain the total volume.

Binding Test. To demonstrate the specific targeting of aptamer and SMNs toward different cell lines, fluorescence measurements were obtained on a FACScan cytometer (Becton Dickinson Immunocytometry Systems, San Jose, CA, USA). A green laser at 488 nm with different excitation voltages (650, 700, and 750 V) was used as the excitation source. Samples containing CEM or Ramos cells with a concentration of 10^6 cells/mL were incubated with the desired concentrations of aptamer or SMN on ice in a 200 μL volume of binding buffer for 30 min. The cells were centrifuged, washed three times with 200 μL of washing buffer, redispersed in 200 μL of binding buffer, and subjected to flow cytometry analysis by counting 10 000 events. The remaining sample after flow cytometry measurement was then directly subjected to confocal fluorescence microscopy.

Internalization and Co-localization Study. To investigate the internalization of aptamers and SMNs into different cell lines, samples containing CEM or Ramos cells with a concentration of 10^6 cells/mL were incubated with the desired concentrations of aptamer or SMN at 37 °C in a volume of 200 μL binding buffer for 2 h with 5% CO_2 atmosphere. The cells were then centrifuged, washed three times with 200 μL of washing buffer, resuspended in 200 μL of binding buffer, and subjected to confocal fluorescence microscopy analysis using an Olympus FV 500-IX81 confocal microscope (Olympus, Center Valley, PA, USA) having a 40× oil-dispersion objective. A 488 nm argon laser was the excitation source for FITC dye, and a 543 nm argon laser was used for the excitation of TAMRA dye. For the co-localization study, 10 μM lysosensor was added for specific staining of the lysosomes of cancer cells during the last 0.5 h of the 2 h incubation. The remaining experimental procedures were the same as those for the internalization study.

Cytotoxicity Assay. The cytotoxicity of SMNs only, DOX-SMNs, or DOX only to CEM and Ramos cells was evaluated using the CellTiter 96 proliferation assay (Promega, Madison, WI, USA). A sample of 1×10^5 cells in 50 μL of fresh cell culture medium was seeded into each test well on a 96-well plate. Then SMNs only, DOX-SMNs, or DOX only (0–2.5 μM) in 50 μL of fresh cell culture medium was added to the test well. The resultant cell mixture was incubated at 37 °C in a 5% CO_2 atmosphere for 2 h. Then, 75 μL cell culture medium was removed from the test well after centrifugation, and another 75 μL of fresh cell culture medium was added. The 96-well plate was then put back into the incubator for another 48 h. Finally, 20 μL CellTiter reagent was added to each test well, and the 96-well plate was subjected to absorption measurement at 490 nm using a VersaMax tunable miroplate reader (Molecular Devices, Inc., Sunnyvale, CA).

Relaxation Measurements and Magnetic Resonance Imaging. T_2 relaxation measurements were carried out at 1.4 T using a standard Carr–Purcell–Meiboom–Gill sequence on a benchtop Minispec mq60 TD-NMR contrast agent analyzer (Bruker Optics, Billerica, MA, USA). SMNs only, SMNs with CEM cells, and SMNs with Ramos cells were incubated on ice for 30 min in 250 μL of PBS buffer in flow tubes. The final concentrations for SMNs and cells were 10 μg/mL and 10^6 cells/mL, respectively. In order to address the concern of SMN aggregation and settling, samples were vortexed for more than 30 s. Then, all the samples were directly transferred into the NMR sample tubes and subjected to T_2 relaxation measurements, without any further washing steps. T_2*-weighted MRI images were taken on a 11 T/470 MHz MRI spectrometer (Bruker Optics, Billerica, MA). SMNs only, SMNs with CEM cells, and SMNs with Ramos cells were incubated on ice for 30 min in 500 μL of PBS buffer in 1.5 mL Eppendorf tubes. The final concentrations for SMNs were 5, 10, 25, and 50 μg/mL, while the final concentration of cells was the same as in the T_2 relaxation measurements. After incubation, the samples in Eppendorf tubes were vortexed, fixed on a homemade foam sample holder in a 4 × 3 array, and then put in the coil. T_2*-weighted MRI images were acquired with a gradient echo sequence (TR = 4000 ms and TE = 20.4 ms).

Acknowledgment. We are grateful to the Interdisciplinary Center for Biotechnology Research (ICBR) at the University of Florida for the TEM technical support and the McKnight Brain Institute at the University of Florida for the MRI technical support. We also sincerely appreciate Dr. Kathryn Williams for her help with manuscript preparation and revision. This work is supported by grants awarded by the National Institutes of Health (GM066137, GM079359, and CA133086), and by the National Key Scientific Program of China (2011CB911000) and China National Grand Program (2009ZX10004-312).

Supporting Information Available: Details of the synthesis and characterization of the heterobifunctional PEG ligand, release kinetics of DOX from DOX-loaded SMNs at different pH values, binding test of SMNs to CEM and Ramos cells using a confocal fluorescence microscope, detailed aptamer sequence information, and cytotoxicity of SMNs only to CEM and Ramos cells. This material is available free of charge *via* the Internet at http://pubs.acs.org.

REFERENCES AND NOTES

1. Poste, G.; Kirsh, R. Site-Specific (Targeted) Drug Delivery in Cancer Therapy. *Nat. Biotechnol.* **1983**, *1*, 869–878.
2. Koo, O.-M.; Rubinstein, I.; Onyuksel, H. Role of Nanotechnology in Targeted Drug Delivery and Imaging: a Concise Review. *Nanomed.: Nanotechnol., Biol., Med.* **2005**, *1*, 193–212.
3. Maeda, H.; Wu, J.; Sawa, T.; Matsumura, Y.; Hori, K. Tumor Vascular Permeability and the EPR Effect in Macromolecular Therapeutics: A Review. *J. Controlled Release* **2000**, *65*, 271–284.
4. Leamon, C. P.; Reddy, J. A. Folate-Targeted Chemotherapy. *Adv. Drug Delivery Rev.* **2004**, *56*, 1127–1141.
5. Park, E.-K.; Kim, S.-Y.; Lee, S.-B.; Lee, Y.-M. Folate-Conjugated Methoxy poly(ethylene glycol)/poly(ε-caprolactone) Amphiphilic Block Copolymeric Micelles for Tumor-Targeted Drug Delivery. *J. Controlled Release* **2005**, *109*, 158–168.
6. Zhang, N.; Chittasupho, C.; Duangrat, C.; Siahaan, T. J.; Berkland, C. PLGA Nanoparticle-Peptide Conjugate Effectively Targets Intercellular Cell-Adhesion Molecule-1. *Bioconjugate Chem.* **2007**, *19*, 145–152.
7. Lo, A.; Lin, C.-T.; Wu, H.-C. Hepatocellular Carcinoma Cell-Specific Peptide Ligand for Targeted Drug Delivery. *Mol. Cancer Ther.* **2008**, *7*, 579–589.
8. Farokhzad, O.-C.; Cheng, J.; Teply, B.-A.; Sherifi, I.; Jon, S.; Kantoff, P.-W.; Richie, J.-P.; Langer, R. Targeted Nanoparticle-Aptamer Bioconjugates for Cancer Chemotherapy *in Vivo*. *Proc. Natl. Acad. Sci.* **2006**, *103*, 6315–6320.

9. Shieh, Y.-A.; Yang, S.-J.; Wei, M.-F.; Shieh, M.-J. Aptamer-Based Tumor-Targeted Drug Delivery for Photodynamic Therapy. *ACS Nano* **2010**, *4*, 1433–1442.
10. Cao, Z.; Tong, R.; Mishra, A.; Xu, W.; Wong, G.-C.-L.; Cheng, J.; Lu, Y. Reversible Cell-Specific Drug Delivery with Aptamer-Functionalized Liposomes. *Angew. Chem., Int. Ed.* **2009**, *48*, 6494–6498.
11. Wu, Y.; Sefah, K.; Liu, H.; Wang, R.; Tan, W. DNA Aptamer-Micelle as an Efficient Detection/Delivery Vehicle Toward Cancer Cells. *Proc. Natl. Acad. Sci.* **2010**, *107*, 5−10.
12. Huang, Y.-F.; Shangguan, D.; Liu, H.; Phillips, J. A.; Zhang, X.; Chen, Y.; Tan, W. Molecular Assembly of an Aptamer−-Drug Conjugate for Targeted Drug Delivery to Tumor Cells. *ChemBioChem* **2009**, *10*, 862–868.
13. Kang, H.; O'Donoghue, M.-B.; Liu, H.; Tan, W. A Liposome-Based Nanostructure for Aptamer Directed Delivery. *Chem. Commun.* *46*, 249−251.
14. Fang, X.; Tan, W. Aptamers Generated from Cell-SELEX for Molecular Medicine: a Chemical Biology Approach. *Acc. Chem. Res.* **2009**, *43*, 48–57.
15. Yoon, Y.; Peisheng, X. Nanoparticles for Tumor-Specific Intracellular Drug Delivery. Engineering in Medicine and Biology Society, 2009. *Annual International Conference of the IEEE*, Sept 3−6, 2009; EMBC, 2009; pp 2403−2405.
16. van Vlerken, L.-E.; Duan, Z.; Seiden, M.-V.; Amiji, M.-M. Modulation of Intracellular Ceramide Using Polymeric Nanoparticles to Overcome Multidrug Resistance in Cancer. *Cancer Res.* **2007**, *67*, 4843–4850.
17. Zhou, J.; Rossi, J.-J. The Therapeutic Potential of Cell-Internalizing Aptamers. *Curr. Top. Med. Chem.* **2009**, *9*, 1144−1157.
18. Tuerk, C.; Gold, L. Systematic Evolution of Ligands by Exponential Enrichment: RNA Ligands to Bacteriophage T4 DNA Polymerase. *Science* **1990**, *249*, 505–510.
19. Ellington, A.-D.; Szostak, J. W. *In Vitro* Selection of RNA Molecules That Bind Specific Ligands. *Nature* **1990**, *346*, 818–822.
20. Jayasena, S.-D. Aptamers: An Emerging Class of Molecules That Rival Antibodies in Diagnostics. *Clin. Chem.* **1999**, *45*, 1628–1650.
21. Shangguan, D.; Li, Y.; Tang, Z.; Cao, Z.-C.; Chen, H. W.; Mallikaratchy, P.; Sefah, K.; Yang, C.-J.; Tan, W. Aptamers Evolved from Live Cells as Effective Molecular Probes for Cancer Study. *Proc. Natl. Acad. Sci.* **2006**, *103*, 11838–11843.
22. Tang, Z.; Shangguan, D.; Wang, K.; Shi, H.; Sefah, K.; Mallikratchy, P.; Chen, H. W.; Li, Y.; Tan, W. Selection of Aptamers for Molecular Recognition and Characterization of Cancer Cells. *Anal. Chem.* **2007**, *79*, 4900–4907.
23. Xiao, Z.; Shangguan, D.; Cao, Z.; Fang, X.; Tan, W. Cell-Specific Internalization Study of an Aptamer from Whole Cell Selection. *Chem.−Eur. J.* **2008**, *14*, 1769–1775.
24. Cammas, S.; Suzuki, K.; Sone, C.; Sakurai, Y.; Kataoka, K.; Okano, T. Thermo-Responsive Polymer Nanoparticles with a Core-Shell Micelle Structure as Site-Specific Drug Carriers. *J. Controlled Release* **1997**, *48*, 157–164.
25. Lu, J.; Choi, E.; Tamanoi, F.; Zink, J.-I. Light-Activated Nanoimpeller-Controlled Drug Release in Cancer Cells. *Small* **2008**, *4*, 421–426.
26. Hu, Y.; Litwin, T.; Nagaraja, A. R.; Kwong, B.; Katz, J.; Watson, N.; Irvine, D. J. Cytosolic Delivery of Membrane-Impermeable Molecules in Dendritic Cells Using pH-Responsive Core-Shell Nanoparticles. *Nano Lett.* **2007**, *7*, 3056–3064.
27. Torchilin, V.-P. Multifunctional Nanocarriers. *Adv. Drug Delivery Rev.* **2006**, *58*, 1532–1555.
28. Sajja, H.-K.; East, M.-P; Mao, H.; Wang, A.-Y; Nie, S.; Yang, L. Development of Multifunctional Nanoparticles for Targeted Drug Delivery and Noninvasive Imaging of Therapeutic Effect. *Curr. Drug Discovery Technol.* **2009**, *6* 43–51.
29. McCarthy, J.-R.; Kelly, K.-A.; Sun, E.-Y; Weissleder, R. Targeted Delivery of Multifunctional Magnetic Nanoparticles. *Nanomedicine* **2007**, *2*, 153–167.
30. Cheng, K.; Peng, S.; Xu, C.; Sun, S. Porous Hollow Fe_3O_4 Nanoparticles for Targeted Delivery and Controlled Release of Cisplatin. *J. Am. Chem. Soc.* **2009**, *131*, 10637–10644.
31. Fritze, A.; Hens, F.; Kimpfler, A.; Schubert, R.; Peschka-Süss, R. Remote Loading of Doxorubicin into Liposomes Driven by a Transmembrane Phosphate Gradient. *Biochim. Biophys. Acta, Biomembr.* **2006**, *1758*, 1633–1640.
32. Sutton, D.; Wang, S.; Nasongkla, N.; Gao, J.; Dormidontova, E.-E. Doxorubicin and β-Lapachone Release and Interaction with Micellar Core Materials: Experiment and Modeling. *Exp. Biol. Med.* **2007**, *232*, 1090–1099.
33. Yang, Y.-J.; Tao, X.; Hou, Q.; Ma, Y.; Chen, X.-L.; Chen, J.-F. Mesoporous Silica Nanotubes Coated with Multilayered Polyelectrolytes for pH-Controlled Drug Release. *Acta Biomater.* *6*, 3092−3100.
34. Giannotti, M.-I.; Esteban, O.; Oliva, M.; García-Parajo, M.-F.; Sanz, F. pH-Responsive Polysaccharide-Based Polyelectrolyte Complexes as Nanocarriers for Lysosomal Delivery of Therapeutic Proteins. *Biomacromolecules* *12*, 2524−2533.
35. Duncan, R. Polymer Conjugates as Anticancer Nanomedicines. *Nat. Rev. Cancer* **2006**, *6*, 688–701.
36. Lee, Y. Biochemistry of Carbohydrate-Protein Interaction. *FASEB J.* **1992**, *6*, 3193–3200.
37. Hong, S.; Leroueil, P.-R.; Majoros, I.-J.; Orr, B.-G.; Baker, J. R., Jr; Banaszak Holl, M.-M. The Binding Avidity of a Nanoparticle-Based Multivalent Targeted Drug Delivery Platform. *Chem. Biol.* **2007**, *14*, 107–115.
38. Perez, J.-M.; Josephson, L.; O'Loughlin, T.; Hogemann, D.; Weissleder, R. Magnetic Relaxation Switches Capable of Sensing Molecular Interactions. *Nat. Biotechnol.* **2002**, *20*, 816–820.
39. Brooks, R. A. T_2-Shortening by Strongly Magnetized Spheres: a Chemical Exchange Model. *Mag. Reson. Med.* **2002**, *47*, 388–391.
40. Gillis, P.; Moiny, F.; Brooks, R.-A. On T_2-Shortening by Strongly Magnetized Spheres: A Partial Refocusing Model. *Magn. Reson. Med.* **2002**, *47*, 257–263.
41. Fellner, F.-A.; Fellner, C.; Aichner, F.-T.; Mölzer, G. Importance of T_2*-Weighted Gradient-Echo MRI for Diagnosis of Cortical Vein Thrombosis. *Eur. J. Radiol.* **2005**, *56*, 235–239.